Atmos. Chem. Phys. Discuss., 4, 7881–7915, 2004
www.atmos-chem-phys.org/acpd/4/7881/
SRef-ID: 1680-7375/acpd/2004-4-7881
European Geosciences Union

Atmospheric Chemistry and Physics Discussions

# Characterisation of the photolytic HONO-source in the atmosphere simulation chamber SAPHIR

**F. Rohrer[1], B. Bohn[1], T. Brauers[1], D. Brüning[1], F.-J. Johnen[1], A. Wahner[1], and J. Kleffmann[2]**

[1]Institut für Chemie und Dynamik der Geosphäre II: Troposphäre, Forschungszentrum Jülich, Jülich, Germany
[2]Physikalische Chemie/FB C, Bergische Universität Wuppertal, Wuppertal, Germany

Received: 11 August 2004 – Accepted: 20 October 2004 – Published: 3 December 2004

Correspondence to: J. Kleffmann (kleffman@uni-wuppertal.de)

## Abstract

HONO formation has been proposed as an important OH radical source in simulation chambers for more than two decades. Besides the heterogeneous HONO formation by the dark reaction of $NO_2$ and adsorbed water, a photolytic source has been proposed to explain the elevated reactivity in simulation chamber experiments. However, the mechanism of the photolytic process is not well understood so far.

As expected, production of HONO and $NO_x$ was also observed inside the new atmosphere simulation chamber SAPHIR under solar irradiation. This photolytic HONO and $NO_x$ formation was studied with a sensitive HONO instrument under reproducible controlled conditions at atmospheric concentrations of other trace gases. It is shown that the photolytic HONO source in the SAPHIR chamber is not caused by $NO_2$ reactions and that it is the only direct $NO_y$ source under illuminated conditions. In addition, the photolysis of nitrate which was recently postulated for the observed photolytic HONO formation on snow, ground, and glass surfaces, can be excluded in the chamber. A photolytic HONO source at the surface of the chamber is proposed which is strongly dependent on humidity, on light intensity, and on temperature. An empirical function of the form $S(HONO)=a_{1,2}\times J(NO_2)\times(1+(RH/RH_0)^2)\times \exp(-T_0/T)$ describes these dependencies and reproduces the observed HONO formation rates to within 10%. It is shown that the photolysis of HONO represents the dominant radical source in the SAPHIR chamber for typical tropospheric $O_3/H_2O$ concentrations. For these conditions, the HONO concentrations inside SAPHIR are similar to recent observations in ambient air.





**ACPD**

4, 7881–7915, 2004

## 1. Introduction

Nitrous acid (HONO) is of particular importance in atmospheric chemistry, since the photolysis of HONO:

$$HONO \xrightarrow{h\nu} NO + OH\,, \qquad \text{(R1)}$$

represents an important OH radical source (Harris et al., 1982; Harrison et al., 1996). Recent studies (Alicke et al., 2002, 2003; Aumont et al., 2003; Ren et al., 2003; Vogel et al., 2003; Zhou et al., 2002a) calculated a significant contribution of the HONO photolysis to the integrated OH yield of up to 60%. Furthermore, HONO is an important indoor pollutant, which can react with amines leading to nitrosamines, which are known to be carcinogenic (Pitts et al., 1978).

Besides in the atmosphere, nitrous acid is also an important precursor for OH radicals in simulation chambers (e.g. Carter et al., 1981), which have been used for many years to study atmospheric chemistry processes. In previous chamber studies a significant OH production was found which could not be attributed to known precursors. To explain this OH production the photolysis of heterogeneously formed HONO was assumed to be responsible, at least in part, for this so called background reactivity in the chambers (Akimoto et al., 1987; Carter et al., 1982; Glasson and Dunker, 1989; Killus and Whitten, 1990; Sakamaki and Akimoto, 1988). It was postulated that HONO is formed by two processes,

a) the heterogeneous dark reaction R2 of $NO_2$ and water (e.g. Carter et al., 1981; Carter et al., 1982; Finlayson-Pitts et al., 2003; Jenkin et al., 1988; Kleffmann et al., 1998; Pitts et al., 1984; Sakamaki et al., 1983; Svensson et al., 1987) responsible for the initiation of photosmog reactions and

$$2NO_2 + H_2O \longrightarrow HONO + HNO_3\,, \qquad \text{(R2)}$$

b) a photoenhanced HONO formation R3 (Akimoto et al., 1987; Glasson and Dunker,

1989; Killus and Whitten, 1990; Sakamaki and Akimoto, 1988; Wang et al., 2000), to explain elevated reactivity under irradiation.

$$Y(HONO) + h\nu \longrightarrow HONO\,. \qquad (R3)$$

The slower process, Reaction 2, was studied and discussed in detail in a recent review article of Finlayson-Pitts et al. (2003) and will not be discussed in the present paper. However, the reaction mechanism of the photoenhanced HONO formation is not well understood, caused by low HONO concentrations under photolysis conditions. In all studies, this process was quantified only indirectly by model calculations. Since in some studies the radical source strength increased with increasing humidity, radiation and with $NO_2$ concentration a photoenhanced reaction of $NO_2$ and water was postulated (Akimoto et al., 1987; Sakamaki and Akimoto, 1988). However, in the study by Glasson and Dunker (1989) no $NO_2$ dependence was observed for the photoenhanced process. Killus and Whitten (1990) compared results from different simulation chambers and postulated that different surface properties might explain the differences. For Teflon surfaces a photoenhanced direct HONO source was postulated by the photolysis of nitrate adsorbed on the surface.

Besides simulation chambers, a photoenhanced HONO formation was recently proposed in the atmosphere over snow (Beine et al., 2001, 2002; Dibb et al., 2002; Honrath et al., 2002; Zhou et al., 2001), ground and vegetation surfaces (Kleffmann et al., 2002, 2003; Ren et al., 2003; Vogel et al., 2003; Zhou et al., 2002a), to explain high day-time concentrations of HONO. The photolytic HONO source was also identified on glass surfaces (Zhou et al., 2002b, 2003) and was explained by the direct photolysis of nitrate/nitric acid and secondary reactions of $NO_2$.

In summary, the photolytic HONO formation, both in the atmosphere and in simulation chambers is not well understood up to now, although it is of significant importance. Accordingly, this process was studied in the atmospheric simulation chamber SAPHIR at atmospheric conditions with a very sensitive HONO instrument. The experimental results were interpreted by box model calculations.

## 2. Experimental

### 2.1. Description of the simulation chamber SAPHIR

The atmospheric simulation chamber SAPHIR (Simulation of Atmospheric PHotochemistry in a large Reaction chamber) is located on the campus of the Forschungszentrum Jülich. It consists of twin wall FEP Teflon foils of 125 $\mu$m and 250 $\mu$m thickness. The space between the twin walls is flushed at all times with high purity air to prevent contamination from outside. The chamber is aligned in north-south direction and has a cylindrical shape with 5 m diameter, 20 m length, and 270 $m^3$ volume. The surface to volume ratio is approximately 1 $m^{-1}$. Synthetic air is prepared by evaporation of high purity (better than 99.9999%) liquid $N_2$ and $O_2$. Exchange of air inside the chamber is done via two flow controller systems. The large one up to 500 $m^3$/h is used to flush the chamber to reach clean starting conditions between experiments. The smaller one up to 15 $m^3$/h is used to replenish the chamber during experiments from losses due to the sampling of instruments and due to leaks. The chamber is operated at approximately 80 Pa overpressure. Under these conditions, the replenishment flow is between 3 and 8 $m^3$/h. Characterisation experiments with NO, $NO_2$, $O_3$, $H_2O$, and other species showed that the replenishment flow causes dilution of trace species inside the chamber which can be described by an exponential decay over more than two orders of magnitude until the detection limits of the instruments are reached. Humidity is introduced into the chamber by heating up high purity water (Milli-Q Gradient A10, Millipore Corp.) and mixing the water vapour to a large flow of synthetic air (300 $m^3$/h) until the desired level of humidity is reached inside the chamber. Therefore the process of humidification up to relative humidities of 80% takes between 30 to 60 min of time. Minimum humidity at a dew point of −50°C or 0.08 mbar of water can be reached when the chamber is flushed more then ten times its volume. The chamber can be exposed to sun light within 60 s by opening a shutter system which also protects the chamber from dangerous weather conditions. Photolysis frequencies inside the chamber are approximately 80% of their outside



ACPD
4, 7881–7915, 2004

values due to shadowing from structural elements holding the shutter system and the Teflon foil. Additionally, a second shutter system equipped with a filter foil can be used to change the spectrum of sun light during exposure. The filter foil almost absorbes all light below 370 nm and has an increasing transmission from <1% to ~85% in the spectral range 370–420 nm. Further details of the chamber will be explained elsewhere (Brauers et al., in preparation, 2004[1]).

### 2.2. Instrumentation

For the measurement of nitrous acid (HONO) a new, very sensitive instrument (LOPAP: Long Path Absorption Photometer) was used, which is described in detail elsewhere (Heland et al., 2001; Kleffmann et al., 2002). Briefly, HONO is sampled in a stripping coil by a fast chemical reaction and converted into an azo dye which is photometrically detected in long path absorption inside a special Teflon tubing. The instrument has an integrated time resolution of ~5 min and a detection limit of 1–2 pptV. Caused by the two-channel concept of the instrument all tested interferences including the combined one against $NO_2$ and unknown semi-volatile diesel exhaust components (Gutzwiller et al., 2002) can be neglected (Kleffmann et al., 2002). In addition, sampling artefacts, such as heterogeneous HONO formation in sampling lines (as an example see, Zhou et al., 2002b), are minimised by the use of an external sampling unit in which the two stripping coils are mounted and which can be placed directly in the atmosphere of interest. In a recent intercomparison campaign with a DOAS instrument in which the same air masses were analysed for the first time (Trick et al., in preparation, 2004[2]) an excellent agreement was obtained also for low concentrations of HONO during daytime. This is

[1] Brauers, T., Johnen, F. J, Häseler, R., Rohrer, F., Bohn, B., Tillmann, R., Rodriguez Bares, S., Wahner, A.: The Atmosphere Simulation Chamber SAPHIR: A Tool for the Investigation of Photochemistry, in preparation, 2004.

[2] Trick, S., Kleffmann, J., Lörzer, J. C., Platt, U., Volkamer, R., and Wiesen, P.: HONO Intercomarison Measurements During the FORMAT campaign in Milan, 2002, in preparation, 2004.

in contrast to intercomparison studies of other chemical detectors with the DOAS technique (Appel et al., 1990; Coe et al., 1997; Febo et al., 1996; Müller et al., 1999), which show large discrepancies during the day probably caused by unknown interferences. The measured and corrected interferences of the LOPAP instrument can account for up to 40% at low HONO concentrations (Trick et al., 2004).

In first measurements the external sampling unit of the LOPAP instrument was directly installed in the SAPHIR chamber. For most of the experiments however, the inlet of the external sampling unit was connected to the northern corner of the chamber by a short PFA tubing (10 cm, 4 mm i.d.). In contrast to complex atmospheric mixtures (Kleffmann et al., 2002), sampling artefacts were found to be small for the low trace gas and relative high HONO concentrations during the experiments in the SAPHIR chamber.

NO and $NO_2$ measurements were performed with a chemiluminescence analyser (ECO PHYSICS TR480) equipped with a photolytic converter (ECO PHYSICS PLC760). The $NO_x$ data were analysed as described by Rohrer et al. (1998). Since HONO mixing ratios were often higher than $NO_2$ mixing ratios in the chamber, the HONO interference of the photolytic conversion system for $NO_2$ is an important factor (for example see Fig. 1). This interference of 15% has been determined experimentally by using a pure HONO source similar to that described by Taira and Kanda (1990) quantified by the LOPAP instrument. Ozone was measured by an UV absorption spectrometer (ANSYCO model O341M). Photolysis frequencies were determined with a spectroradiometer (as described by Hofzumahaus et al., 1999) on the roof of the building beside the SAPHIR chamber. To account for shadowing effects of structural elements of the chamber, the photolysis frequency data were corrected with the help of numerical calculations (Bohn and Zilken, 2004; Bohn et al., 2004[3]). Humidity was determined with a frost point hygrometer (General Eastern model Hygro M4) and air

[3]Bohn, B., Rohrer, F., Brauers, T., and Wahner, A.: Photolysis Frequencies in a Sun Lit Simulation Chamber, Part 2: Actinometry and Radiometry, Atmos. Chem. Phys. Discuss., submitted, 2004.



ACPD
4, 7881–7915, 2004

temperature by an ultra sonic anemometer (Metek USA-1, accuracy 0.3 K).

Several cross checks of the instrumentation were performed to examine the consistency of the data sets. The pure HONO source was analysed by the LOPAP instrument and by the $NO_x$ instrumentation by using a catalytic conversion system for $NO_y$ as described by Fahey et al. (1985). Both instruments showed agreement within 5%. A second test was performed by introducing 50 ppbV of $NO_2$ into the chamber with closed shutters. After exposure to sunlight and photolysis of $NO_2$ yielding equal amounts of NO and ozone, the NO and ozone instruments showed consistency within 2%. Moreover, the photostationary state of NO, ozone, and $NO_2$ reached after exposure with light was consistent within 10% with the measured photolysis frequency $J(NO_2)$ and the recommended literature value for the rate constant of the reaction of NO with ozone (Sander et al., 2003).

## 3. Measurement Concept

The illuminated atmosphere simulation chamber SAPHIR generates HONO, $NO_x$, and $O_3$. For most experimental conditions the HONO concentration originating from this process is large enough so that OH production via HONO photolysis is significant for the interpretation of simulation experiments. Therefore, a series of dedicated experiments has been designed to determine reproducibility and dependencies on boundary conditions for the characterization of HONO and $NO_x$ production in SAPHIR. These experiments consist of three parts: a) preparation of initial conditions, b) illumination with solar irradiation, and c) interpretation of results. The preparation of initial conditions is started by flushing the chamber with high purity air for a long enough time so that all measured species are close to their detection limit. For some of the experiments relative humidity, CO, or $NO_x$ concentrations are adjusted to preselected values to determine the production rates of HONO and $NO_x$ for these conditions. Temperature in SAPHIR can not be adjusted. Variation of temperature is therefore limited to natural variability. When initial conditions are adjusted, the roof of the chamber is opened so



ACPD
4, 7881–7915, 2004

that the air sample in the chamber is illuminated. The time series of $NO_x$, $O_3$, humidity, temperature, and of photolysis frequencies are monitored for all of these experiments. The variation of HONO is measured also for some of the experiments depending on availability of the detection system. After a few hours of solar illumination, the roof is closed finishing the experiment. The interpretation of the experiments is done with the help of a photochemical model. The parameters of the model describing the generation of HONO are adjusted so that the measured time responses of $NO_x$ and $O_3$ are reproduced. If available the measured HONO concentrations are also used to check for consistency with model assumptions. With several of these experiments at hand, common features like the dependence on humidity or on solar irradiation are parameterized so that as many of these experiments as possible can be described with a parameterization as simple as possible. The key feature of this concept is reproducibility. For this reason these dedicated experiments have to be repeated at regular intervals.

## 4. Results

### 4.1. Dedicated experiments in the SAPHIR chamber

For most of the experiments presented here, the SAPHIR chamber was flushed by synthetic air over night until the trace gas concentrations were below the detection limits of the instruments. Afterwards, initial conditions for humidity were adjusted. When the SAPHIR chamber was exposed to sun light the instantaneous formation of HONO and other trace gases like NO, $NO_2$, and $O_3$ was observed (see Figs. 1 and 2). For "clean" conditions, no formation of these trace species was observed without illumination. But in several experiments (for example Fig. 1), small amounts of HONO and $NO_2$ were detected in the dark chamber associated only with the process of humidification. This artefact was observed when the humidifier was not in operation for a longer time. It is probably due to impurities of nitrite compounds adsorbed on the walls of the water injection system, which are hydrolysed and flushed into the chamber. In some of the



ACPD
4, 7881–7915, 2004

experiments, 550 ppmV of CO were injected into the chamber to suppress OH concentrations below $10^4$ cm$^{-3}$. Under these conditions, the interpretation of the budgets of $NO_x$ and HONO was very much simplified because only production of HONO, photolysis of HONO and dilution of HONO and $NO_x$ had to be taken into account. In a single dedicated experiment, 30% relative humidity and an initial $NO_2$ mixing ratio of 35 ppbV were used to search especially for a $NO_2$ enhanced HONO formation. Overall, 5 different experimental conditions summarised in Table 2 were used to characterise HONO emissions in SAPHIR in the time period between July 2001 and December 2003.

In these experiments, typical HONO concentrations were under irradiation in the region of several 100 pptV for high humidities of >10% RH and several 10 pptV for low humidities at dew points of −40°C. The dominat influence of irradiation and humidity on HONO production rates was therefore obvious. To further study the photoenhanced HONO formation in the SAPHIR chamber, the spectral range of the radiation inside the chamber was varied. For this purpose HONO formation was studied under humid condition when light at short wavelengths (<370 nm) was absorbed outside the Teflon chamber by the use of the filter foil. In the spectral range 370–420 nm, the transmission of the filter foil increases from <1% to ∼85%. Accordingly, the photolysis frequency of $NO_2$, $J(NO_2)$, decreased by a factor of ∼3 by the filter foil, J(HONO) by a factor of 10, and the photolysis frequency of ozone, $J(O^1D)$, decreased by a factor of 100. Nevertheless, when the filter foil was used, still a significant HONO formation was observed under irradiation (see Fig. 2).

### 4.2. Model calculations

In order to quantify the HONO production rate $S(HONO)_{SAPHIR}$ under various conditions model calculations were performed using the photochemical reaction scheme outlined in Table 3 describing a simple $NO_x$/HONO/CO/HCHO chemistry with reaction constants taken from Sander et al. (2003). In addition to Reaction (3) (see Introduction), Reactions (4–6) were introduced into the model to account for several phenom-



ACPD
4, 7881–7915, 2004

ena observed in SAPHIR:

| | | | |
|---|---|---|---|
| OH + X | $\longrightarrow HO_2$ | k=k(CO + OH) | (R4) |
| all tracers | $\longrightarrow$ | k=flow/volume | (R5) |
| Y(HCHO) + hv | $\longrightarrow$ HCHO | rate:0–0.2 ppbV/h | (R6) |

Reaction (3) describes the observation of photolytically induced HONO and succeeding NO, and $NO_2$ formation. In addition, to simulate the small increases of $NO_2$ and HONO during some humidification processes in the dark chamber, appropriate amounts of $NO_2$ and HONO were introduced into the model calculations also (see Fig. 1). These small amounts of HONO do not play a significant role, because they are photolysed in 10 to 20 min when the chamber is illuminated. Reaction 4 accounts for the phenomenon that even with very clean starting conditions when all measured NMHC's are below their detection limit immediate ozone formation is observed when the chamber is illuminated. All measured species like CO and NMHC's are below their detection limits at the beginning of the experiments. For this reason an unknown species X was indroduced in the chemical mechanism which can react with OH giving $HO_2$. Subsequent reaction of $HO_2$ with NO gives the desired ozone formation. To facilitate comparisons, the reaction constant of CO with OH from Sander et al. (2003) was used as a parameter for Reaction (4). Reactions similar to Reaction (5) were introduced for all trace species in the reaction mechanism to describe dilution by the replenishment flow as first order loss reactions. The reaction constant was calculated from the volume of the chamber and the measured replenishment flow. Reaction (6) is necessary to follow the observed HCHO production when the chamber is illuminated. The HCHO formation was linear with time and depending on humidity, light intensity and temperature. The rate of HCHO formation used in the model was adjusted to the measured rate. However, this reaction has only marginal influence on the $HO_x$ budget in the chamber and is given here only for completeness. The characterisation of the HCHO source in the SAPHIR chamber will be described in a forthcoming paper.



ACPD
4, 7881–7915, 2004

Subsequent model calculations showed that the following empirically derived parameterisation for the production rate of HONO describes the observed time series of NO and $NO_2$:

$$S(HONO)_{SAPHIR,i} = a_i \times J(NO_2) \times (1 + (RH/RH_0)^2) \times e^{-T_0/T} \qquad i=1,2. \tag{1}$$

T represents the temperature, RH the relative humidity , $J(NO_2)$ the photolysis frequency of $NO_2$ and $a_i$, $RH_0$ and $T_0$ are fitting parameters specified in Table 4. Equation (1) is an empirical function with only three parameters which is able to describe the HONO formation in SAPHIR with good precision for a broad band of boundary conditions. This is a significant step forward in the process of using the simulation chamber SAPHIR as a tool for atmospheric chemistry. Equation (1) is not based on a physical model of processes controlling HONO formation in SAPHIR.

To find the optimum set of parameters for Eq. (1), humidity, temperature, and $J(NO_2)$ were used as observed. The concentrations of the unknown species X for Reaction (4) were chosen independently for each experiment to explain the measured ozone concentrations. The value of X varied between 100 and 300 ppbV of CO equivalents. Its variation could not be attributed to a certain process.

The parameters $a_i$, $RH_0$ and $T_0$ were then optimised by fitting the observed NO and $NO_2$ mixing ratios of the experiments mentioned in Table 2 to model calculations with the help of the Levenberg-Marquard algorithm. The results of these calculations are shown in Figs. 1 and 2 as red lines. The green lines describe the calculated $NO_2$ time series including 15% of the calculated HONO mixing ratios to account for the HONO interference of the detection system for $NO_2$ (see Sect. 2.2). Two sets of parameters were determined. The experiments before August 2002 could be explained by one set of parameters, the experiments after that date by another set of parameters. The parameters $a_1$ and $a_2$ describe the difference between both sets of experiments which is a factor of 1.8. The time frame for this change is defined by the experiments of 9 July and 13 August 2002. Between these limiting HONO experiments, several other experiments were performed in the chamber namely ozonolysis of alkens and actinometric



ACPD
4, 7881–7915, 2004

experiments with 30 ppbV of $NO_2$. But these types of experiments were also conducted before and after that time frame. Therefore the reason for the sudden change in the photoenhanced emission rate of HONO remains unknown. Table 4 summarises these results.

Figure 3 shows the result of the optimisation process for the experiments with relative humidities of less than 1%. Both sets of experiments are clearly distinguishable. The estimated uncertainty of the determination of a single HONO production rate of 0.15 is shown here as the vertical line at each data point. Horizontal lines mark the temperature range covered by each experiment.

Figure 4 shows the result of the optimisation process for the experiments started with relative humidities of more than 10%. As in Fig. 3, both groups of experiments are clearly visible. Interestingly, experiments with 550 ppmV CO or with the filter foil cannot be identified in the plot. The values calculated with Eq. (1) with both sets of parameters in Table 4 are included in Fig. 4 as solid black lines. Dotted lines mark regions which are defined by the envelope embedding all of the individual experiments. This maximum spread of experiments in both groups is ±15%. The accuracy of Eq. (1) is therefore estimated to be on the order of 10%.

## 5. Discussion

In other studies, a photoenhanced background reactivity was proposed to explain elevated reactivity in simulation chambers under irradiation (Akimoto et al., 1987; Glasson and Dunker, 1989; Killus and Whitten, 1990; Sakamaki and Akimoto, 1988; Wang et al., 2000). However, in contrast to all known studies of the background reactivity of simulation chambers, HONO was unequivocally identified under illuminated conditions in the present study for the first time. The photolytic HONO source in SAPHIR was found to be proportional to the photolysis frequency of $NO_2$, which is in good agreement with parameterisations of the background reactivity made in the study of Wang et al. (2000). In addition, the photolytic HONO source increased with the square of relative humidity



ACPD
4, 7881–7915, 2004

and exponentially with temperature. A water dependence of the background reactivity was also observed in most other studies (Akimoto et al., 1987; Killus and Whitten, 1990; Sakamaki and Akimoto, 1988). The excellent agreement between experimental results and model calculation clearly shows that the photolytic HONO source is the dominant $NO_x$ source in the chamber, in good agreement with suggestions of Killus and Whitten (1990). In contrast, a direct photolytic $NO_x$ source which has recently be proposed for snow (Davis et al. 2001; Honrath et al., 1999, 2000; Jones et. al., 2000, 2001) and glass surfaces (Zhou et al., 2002b, 2003) by the photolysis of nitrate can be excluded, since the modelled HONO concentration would be significantly higher than the measured one in this case.

In two older studies (Akimoto et al., 1987; Sakamaki and Akimoto, 1988), the elevated reactivity in simulation chambers under irradiation was explained by a photoenhancement of Reaction (2), $2NO_2+H_2O$, since the radical source strength increased with increasing humidity, radiation and $NO_2$ concentration. However, a photoenhancement of Reaction (2) can be clearly excluded based on the results of the present study, since the majority of experiments started with very low $NO_2$ concentrations on the order of 20 pptV $NO_2$ or less. During the course of these experiments, $NO_2$ increased to several 100 pptV without influence on the photolytic HONO formation. In a dedicated experiment (experiment type E, Table 2), 35 ppbV of $NO_2$ at 30% relative humidity were used as starting conditions again showing no enhancement on the photolytic HONO production. Taking everything together, these experiments showed that a photoenhancement of the reaction of $NO_2$ with water vapor, Reaction (2), was not observed in SAPHIR.

In the study of Killus and Whitten (1990) the photoenhancement of the background reactivity in Teflon chambers was explained by the photolysis of nitrate, since elevated reactivity was observed after experiments in which high nitric acid concentrations were used. The photolysis of nitrate as a source of HONO was recently also proposed in the atmosphere over snow (Beine et al., 2001, 2002; Dibb et al., 2002; Honrath et al., 2002; Zhou et al., 2001), ground and vegetation surfaces (Zhou et al., 2002a), to

explain high day-time concentrations of HONO. In addition, a photolytic HONO source by photolysis of nitrate was proposed for glass surfaces (Zhou et al., 2002b, 2003). However, based on the results from the present study, the photolysis of nitrate can be excluded. A significant HONO formation was also observed in SAPHIR when light with wavelengths <370 nm was blocked by the filter foil. Since the weak absorption band of nitrate at ~300 nm ($\varepsilon$=~7 l mol$^{-1}$ cm$^{1}$, Meyerstein and Treinin, 1961) was found to be responsible for nitrite and $NO_2$ formation in solution (Wagner et al., 1980), and since nitrate absorption does not extend to wavelengths >370 nm, no significant photolytic HONO formation would have been expected in the experiments with the filter foil. In the present study a good correlation of the photolytic HONO formation with the photolysis frequency of $NO_2$ was found. Accordingly, it is expected that the precursor of HONO absorbs in a similar wavelength range compared to $NO_2$. In contrast, absorption at wavelengths exclusively <370 nm and exclusively >420 nm can be excluded, since HONO formation should have been reduced by two orders of magnitude in the first case and only by 15% in the second case, caused by the transmission of the filter foil.

In a recent study of Saliba et al. (2001) it was shown by infrared spectroscopy that adsorbed nitric acid should be almost undissociated on surfaces up to a water coverage of the surface of three formal monolayers. However, photolysis of adsorbed $HNO_3$ can only explain the experimental observations, if the relative shape of the UV absorption spectra of undissociated adsorbed $HNO_3$ is significantly different to the spectra of undissociated gaseous $HNO_3$ (Sander et al., 2003). The UV absorption cross section of $HNO_3/H_2O$ films on $Al_2O_3$ surfaces was recently measured by Berland et al. (1996). Unfortunately, only the $\pi \rightarrow \pi^*$ band at ~200 nm was investigated. For the oscillator strength of the band no significant difference between thin films of nitric acid and gaseous nitric acid was observed. In addition, the band was shifted by only ~10 nm to longer wavelength for the thin film. Accordingly, it can be concluded that adsorbed undissociated $HNO_3$ has a similar UV absorption spectra compared to gaseous nitric acid. As an upper limit of the long wavelength photolysis of adsorbed $HNO_3$ in the spectral range of the SAPHIR chamber, it was assumed that the absorption cross sec-



ACPD
4, 7881–7915, 2004

tion of adsorbed $HNO_3$ is similar to that of gaseous $HNO_3$ given by Sander et al. (2003) and remains constant in the wavelength range 350–420 nm with the lowest value given for gaseous $HNO_3$ for 350 nm. Under this assumption, HONO formation by photolysis of adsorbed $HNO_3$ should be reduced by a factor of >50 by the use of the filter foil. However, only a reduction of a factor of 3 was observed in the experiments. In addition, by using the obviously overestimated absorption cross sections mentioned above, a $HNO_3$ adsorption of 10 monolayers, which is an unrealistic high value for the SAPHIR chamber and a quantum yield of 1 for HONO formation by $HNO_3$ photolysis, which is two orders of magnitude higher than the effective quantum yield for nitrite formation by nitrate photolysis in solution at pH 4–7 (Mark et al., 1996), the rate of HONO formation in the chamber would be still more than one order of magnitude lower than the measured one in the experiments with the filter foil. Another argument against the photolysis of adsorbed undissociated $HNO_3$ is the observation, that photolytic HONO formation still increased for relative humidities of >50%. For the highest relative humidities of ~80% it can be expected, that $HNO_3$ will dissociate to nitrate (Saliba et al., 2001; Svensson and Ljungström, 1987), which was excluded as a precursor of HONO in the chamber (see above). Accordingly, it is proposed that adsorbed nitric acid does not represent the precursor of HONO formed during the irradiation of the chamber, although this cannot be completely excluded, since the UV absorption spectra of adsorbed nitric acid on Teflon surfaces is unknown.

In the study of Killus and Whitten (1990) elevated background reactivity was documented for Teflon chambers after experiments with high nitric acid concentrations. Based on these results it might be possible that the precursor of HONO is formed by a reaction of $HNO_3$ with unknown compounds in the fibre structure of the Teflon foil. Candidates for these compounds might be higher molecular organics from the production of the Teflon material, which are oxidised by $HNO_3$. From the experiments with the filter foil it can be concluded that the precursor of HONO should photolyse in a similar wavelength range than $NO_2$. In contrast it cannot photolyse in the spectral range in which nitrate or gaseous $HNO_3$ absorb.



ACPD
4, 7881–7915, 2004

The water dependence of the photolytic HONO source was described by a quadratic function (see Eq. 1), which resembles the dependence of water uptake on FEP Teflon shown in Fig. 7 of Svensson et al. (1987). Based on the observed humidity dependence of the photolytic HONO source it can be speculated that either only the dissociated form of the precursor photolyses or that HONO is formed by a reaction of photolysis products with adsorbed water. One candidate might be a hypothetical fast reaction of an excited $NO_2$ molecule, formed in the photolysis of the unknown precursor, with water. In contrast, the reaction of ground state $NO_2$ molecules with adsorbed water cannot explain the experimental findings, since no enhancement of the photolytic HONO formation was observed with increasing $NO_2$ concentration. Since it is well known that molecules diffuse through Teflon material, it can be expected that $HNO_3$ will react with the postulated organic compounds also on the internal surface of the Teflon foil. Since $HNO_3$ is formed as the end product of $NO_x$ in the most of the experiments and since efficient deposition of $HNO_3$ on the wall can be expected, the concentration of the precursor and accordingly the photolytic HONO source will probably not decrease significantly, as observed over a period of more than two years in the chamber. However, this argument holds only, if the concentration of the speculated organic compound, which forms the precursor of HONO by reaction with $HNO_3$, is high enough. However, to quantitatively explain photolytic HONO formation in the SAPHIR chamber in 100 experiments only a fraction of $\sim 10^{-5}$ of a hypothetical compound in the Teflon foil with an assumed molecular mass of 500 amu is needed, which is reasonable.

In conclusion, although several pathways of the photolytic HONO formation discussed in the literature could be excluded, e.g. a photoenhancement of the reaction of $NO_2$ and $H_2O$ or a photolysis of nitrate, the precursor of HONO formed photolytically in the SAPHIR chamber was not identified. Accordingly further work is needed to clarify this process which is of paramount importance for the radical balance of simulation chambers.

It was shown that HONO production in the simulation chamber SAPHIR can be predicted with good precision. This prediction capability can now be used to characterise



ACPD
4, 7881–7915, 2004

the radical production in SAPHIR and compare it to radical production in ambient air to show that SAPHIR is a suitable tool for atmospheric simulation experiments at ambient conditions. If the photolytic production of HONO (Reaction 3) is the dominant source and the photolysis of HONO (Reaction 1) the dominant sink of HONO in the SAPHIR chamber, then a simple photostationary state calculation of HONO can be performed:

$$[\mathrm{HONO}] = \frac{P(\mathrm{HONO})}{J(\mathrm{HONO})} = \frac{S(\mathrm{HONO})_{\mathrm{SAPHIR}}}{J(\mathrm{HONO})} \quad (2)$$

Taking into account the strong correlation between $J(NO_2)$ and $J(HONO)$ (Kraus and Hofzumahaus, 1998), the steady state concentration of HONO can be calculated:

$$J(\mathrm{HONO}) = J(\mathrm{NO_2})/5.8 \quad (3)$$

$$[\mathrm{HONO}]_i = a_i \times 5.8 \times (1 + (\mathrm{RH}/\mathrm{RH}_0)^2) \times e^{-T_0/T} \quad (4)$$

$$P(\mathrm{OH})_{\mathrm{HONO}} = [\mathrm{HONO}]_i \times J(\mathrm{HONO}) = S(\mathrm{HONO})_i \,. \quad (5)$$

Equation (4) was used to calculate steady state HONO concentrations for different humidities at 295 K in the SAPHIR chamber. The results are shown in Fig. 5. These calculations emphasise the difference between the two parameters $a_1$ and $a_2$ in Table 4 which distinguish between the time before August 2002, and afterwards. The calculated mixing ratios are in good agreement with LOPAP HONO measurements. Using typical values for $J(NO_2)$ and $J(O^1D)$ of $5\times10^{-3}\,s^{-1}$ and $1.5\times10^{-5}\,s^{-1}$ respectively, Eqs. (1) and (5) can be used to compare the production of OH from HONO photolysis to the production rate from ozone photolysis $P(OH)_{O_3}$, Eq. (6), determined by Reactions (7–10):

$$P(\mathrm{OH})_{\mathrm{O_3}} = \frac{2 \times [\mathrm{O_3}] \times J(\mathrm{O^1D}) \times k_8 \times [\mathrm{H_2O}]}{k_8 \times [\mathrm{H_2O}] + k_9 \times [\mathrm{N_2}] + k_{10} \times [\mathrm{O_2}]} \quad (6)$$

$$\mathrm{O_3} + h\nu \longrightarrow \mathrm{O^1D} + \mathrm{O_2} \quad (R7)$$



ACPD
4, 7881–7915, 2004

$$O^1D + H_2O \longrightarrow 2OH \quad \text{(R8)}$$

$$O^1D + N_2 \longrightarrow O^3P + N_2 \quad \text{(R9)}$$

$$O^1D + O_2 \longrightarrow O^3P + O_2\,. \quad \text{(R10)}$$

With steady-state concentrations of HONO taken from Fig. 5, the OH production from HONO photolysis is compared to OH production rates calculated with typical tropospheric ozone concentrations of 50 and 100 ppbV in Fig. 6. The total OH production in SAPHIR for these illumination conditions is in the region of 1 to $30\times10^6$ cm$^{-3}$ s$^{-1}$ or 150–4500 pptV/h. In the range 5% to 30% relative humidity, both processes have approximately the same contribution. Above 60% or below 5% relative humidity, OH production by HONO photolysis is 2 to 6 times larger than by ozone photolysis.

The calculated HONO concentrations and OH production rates can be compared to ambient measurements. Recent studies show HONO mixing ratios in the range 50–500 pptV (Kleffmann et al., 2002, 2003; Ren et al., 2003; Zhou et al., 2002a) during daylight. In addition OH production rates of 200–1800 pptV/h were estimated for the atmosphere (Ren et al., 2003; Zhou et al., 2002a). This comparison shows, that HONO photolysis is comparable to or dominating the OH production from ozone photolysis inside the SAPHIR chamber but also outside in ambient air (e.g. Ren et al., 2003; Vogel et al., 2003).

## 6. Summary

It was shown that the photoenhanced HONO production in the simulation chamber SAPHIR depends exclusively on solar irradiation, relative humidity, and temperature. The rate of HONO productions can be predicted with good precision by an empirical parameterisation including the photolysis frequency of $NO_2$, $J(NO_2)$, as a scaling factor for solar irradiation, a square dependence on relative humidity, and exponential growth with temperature. Photolysis of HONO seems to be the only source of NO and

OH in the flushed-out simulation chamber. The good reproducibility of the HONO production rate and its independence on other boundary conditions, especially on $NO_2$ concentration, allows the inclusion of this process in further studies which depend on the quantitative understanding of the $HO_x$ radical budget or the nitrogen oxide budget.

*Acknowledgements.* This work was supported by the BMBF German Atmospheric Research Program AFO2000, within its subproject IDEC (Integrated Data Archive of Atmospheric Chemical Standard Scenarios for the Evaluation of Chemistry-Transport Models) under grant 07ATF02.

## References

Akimoto, H., Takagi, H., and Sakamaki, F.: Photoenhancement of the Nitrous Acid Formation in the Surface Reaction of Nitrogen Dioxide and Water Vapour: Extra Radical Source in Smog Chamber Experiments, Int. J. Chem. Kinet., 19, 539–551, 1987.

Alicke, B., Platt, U., and Stutz, J.: Impact of Nitrous Acid Photolysis on the Total Hydroxy Radical Budget During the Limitation of Oxidant Production/Pianura Padana Produzione di Ozono Study in Milan, J. Geophys. Res., 107 (D22), 8196, doi:10.1029/2000JD000075, 2002.

Alicke, B., Geyer, A., Hofzumahaus, A., Holland, F., Konrad, S., Pätz., H. W., Schäfer, J., Stutz, J., Volz-Thomas, A., and Platt, U.: OH Formation by HONO Photolysis During the BERLIOZ Experiment, J. Geophys. Res., 108 (D4), 8247, doi:10.1029/2001 JD000579, 2003.

Appel, B. R., Winer, A. M., Tokiwa, Y., and Biermann, H. W.: Comparison of Atmospheric Nitrous Acid Measurements by Annular Denuder and Optical Absorption Systems, Atmos. Envir., 24 A, 611–616, 1990.

Aumont, B., Chervier, F., and Laval, S.: Contribution of HONO Sources to the $NO_x/HO_x/O_3$ Chemistry in the Polluted Boundary Layer, Atmos. Envir., 37, 487–498, 2003.

Beine, H. J., Allegrini, I., Sparapani, R., Ianniello, A., and Valentini, F.: Three Years of Springtime Trace Gas and Particle Measurements at Ny-Ålesund, Svalbard, Atmos. Envir., 35, 3645–3658, 2001.

Beine, H. J., Dominé, F., Simpson, W., Honrath, R. E., Sparapani, R., Zhou, X., and King, M.: Snow-pile and Chamber Experiments during the Polar Sunrise Experiment, Alert 2000: Exploration of Nitrogen Chemistry, Atmos. Envir., 36, 2707–2719, 2002.

Berland, B. S., Foster, K. L., Tolbert, M. A., and George, S. M.: UV Absorption Spectra of $H_2O/HNO_3$ Films, Geophys. Res. Lett., 23, 2757–2760, 1996.
Bohn, B. and Zilken, H.: Model-aided radiometric determination of photolysis frequencies in a sunlit atmosphere simulation chamber, Atmos. Chem. Phys. Discuss., 4, 6967–7010, 2004, SRef-ID: 1680-7375/acpd/2004-4-6967.
Carter, W. P. L., Atkinson, R., Winer, A. M., and Pitts Jr., J. N.: Evidence for Chamber-Dependent Radical Source: Impact on Kinetic Computer Models for Air Pollution, Int. J. Chem. Kinet., 13, 735–740, 1981.
Carter, W. P. L., Atkinson, R., Winer, A. M., and Pitts Jr., J. N.: Experimental Investigation of Chamber-Dependent Radical Source, Int. J. Chem. Kinet., 14, 1071–1103, 1982.
Coe, H., Jones, R. L., Colin, R., Carleer, M., Harrison, R. M., Peak, J., Plane, J. M. C., Smith, N., Allan, B., Clemitshaw, K. C., Burgess, R. A., Platt, U., Etzkorn, T., Stutz, J., Pommereau, J.-P., Goutail, F., Nunes-Pinharanda, M., Simon, P., Hermans, C., and Vandaele, A.-C.: A Comparison of Differential Optical Absorption Spectrometers for Measurement of $NO_2$, $O_3$, $SO_2$ and HONO, in: Proceedings of EUROTRAC Symposium '96: Transport and Transformation of Pollutants, edited by: Borrell, P. M., Borrell, P., Cvitaš, T., Kelly, K., Seiler, W., ISBN 1-85312-498-2, Computational Mechanics Publications, Southampton, 757–762, 1997.
Davis, D., Nowak, J. B., Chen, G., Buhr, M., Arimoto, R., Hogan, A., Eisele, E., Mauldin, L., Tanner, D., Shetter, R., Lefer, B., and McMurry, P.: Unexpected High Levels of NO Observed at South Pole, Geophys. Res. Lett., 28, 3625–3628, 2001.
Dibb, J. E., Arsenault, M., Peterson, M. C., and Honrath, R. E.: Fast Nitrogen Oxide Photochemistry in Summit, Greenland Snow, Atmos. Envir., 36, 2501–2511, 2002.
Fahey, D. H., Eubank, C. S., Hübler, G., and Fehsenfeld, F. C.: Evaluation of a Catalytic Reduction Technique for the Measurement of Total Reactive Odd-Nitrogen $NO_y$ in the Atmosphere, J. Atmos. Chem., 3, 435–468, 1985.
Febo, A., Perrino, C., and Allegrini, I.: Measurement of Nitrous Acid in Milan, Italy, by DOAS and Diffusion Denuders, Atmos. Envir., 30, 3599–3609, 1996.
Finlayson-Pitts, B. J., Wingen, L. M., Sumner, A. L., Syomin, D., and Ramazan, K. A.: The Heterogeneous Hydrolysis of $NO_2$ in Laboratory Systems and in Outdoor and Indoor Atmospheres, An Integrated Mechanism, Phys. Chem. Chem. Phys., 5, 223–242, 2003.
Glasson, W. A. and Dunker, A. M.: Investigation of Background Radical Sources in a Teflon-Film Irradiation Chamber, Environ. Sci. Technol., 23, 970–978, 1989.
Gutzwiller, L., Arens, F., Baltensperger, U., Gäggeler, H. W., and Ammann, M.: Significance of

Semivolatile Diesel Exhaust Organics for Secondary HONO Formation, Environ. Sci. Technol., 36, 677–682, 2002.
Harris, G. W., Carter, W. P. L., Winer, A. M., Pitts Jr., J. N., Platt, U., and Perner, D.: Observation of Nitrous Acid in the Los Angeles Atmosphere and Implications for Predictions of Ozone-Precursor Relationships, Environ. Sci. Technol., 16, 414–419, 1982.
Harrison, R. M., Peak, J. D., and Collins, G. M.: Tropospheric Cycle of Nitrous Acid, J. Geophys. Res., 101, 14 429–14 439, 1996.
Heland, J., Kleffmann, J., Kurtenbach, R., and Wiesen, P.: A New Instrument to Measure Gaseous Nitrous Acid (HONO) in the Atmosphere, Environ. Sci. Technol., 35, 3207–3212, 2001.
Hofzumahaus, A., Kraus, A., and Müller, M.: Solar Actinic Flux Spectroradiometry: A New Technique to Measure Photolysis Frequencies in the Atmosphere, Appl. Opt., 38, 4443–4460, 1999.
Honrath, R. E., Peterson, M. C., Guo, S., Dibb, J. E., Shepson, P. B., and Campbell, B.: Evidence of $NO_x$ Produduction within or upon Ice Particles in the Greenland Snowpack, Geophys. Res. Lett., 26, 695–698, 1999.
Honrath, R. E., Guo, S., Peterson, M. C., Dziobak, M. P., Dibb, J. E., and Arsenault, M. A.: Photochemical Production of Gas Phase $NO_x$ from Ice Crystal $NO_3^-$, J. Geophys. Res., 105, 24 183–24 190, 2000.
Honrath, R. E., Y. Lu, Peterson, M. C., Dibb, J. E., Arsenault, M. A., Cullen, N. J., and Steffen, K.: Vertical Fluxes of $NO_x$, HONO, and $HNO_3$ above the Snowpack at Summit, Greenland, Atmos. Envir., 36, 2629–2640, 2002.
Jenkin, M. E., Cox, R. A., and Williams, D. J.: Laboratory Studies of the Kinetics of Formation of Nitrous Acid from the Thermal Reaction of Nitrogen Dioxide and Water Vapour, Atmos. Envir., 22, 487–498, 1988.
Jones, A. E., Weller, R., Wolff, E. W., and Jacobi, H.-W.: Speciation and Rate of Photochemical NO and $NO_2$ Production in Antarctic Snow, Geophys. Res. Lett., 27, 345–348, 2000.
Jones, A. E., Weller, R., Anderson, P. S., Jacobi, H.-W., Wolff, E. W., Schrems, O., and Miller, H.: Measurements of $NO_x$ Emissions from the Antarktic Snowpacks, Geophys. Res. Lett., 28, 1499–1502, 2001.
Killus, J. P. and Whitten, G. Z.: Background Reactivity in Smog Chambers, Int. J. Chem. Kinet., 22, 547–575, 1990.
Kleffmann, J., Becker, K. H., and Wiesen, P.: Heterogeneous $NO_2$ Conversion Processes on

Acid Surfaces: Possible Atmospheric Implications, Atmos. Envir., 32, 2721–2729, 1998.
Kleffmann, J., Heland, J., Kurtenbach, R., Lörzer, J. C., and Wiesen, P.: A New Instrument (LOPAP) for the Detection of Nitrous Acid (HONO), Environ. Sci. Pollut. Res., 9 (special issue 4), 48–54, 2002.
Kleffmann, J., Kurtenbach, R., Lörzer, J. C., Wiesen, P., Kalthoff, N., Vogel, B., and Vogel, H.: Measured and Simulated Vertical Profiles of Nitrous Acid, Part I: Field Measurements, Atmos. Envir., 37, 2949–2955, 2003.
Kraus, A. and Hofzumahaus, A.: Field Measurements of Atmospheric Photolysis Frequencies for $O_3$, $NO_2$, HCHO, $CH_3CHO$, $H_2O_2$, and HONO by UV Spectroradiometry, J. Atmos. Chem., 31, 161–180, 1998.
Mark, G., Korth, H.-G., Schuchmann, H.-P., and von Sonntag, C.: The Photochemistry of Aqueous Nitrate Ion Revised, Photochem. Photobiol., 101, 89–103, 1996.
Meyerstein, D. and Treinin, A.: Absorption Spectra of $NO_3^-$ in Solution, Trans. Faraday Soc., 57, 2104–2112, 1961.
Müller, Th., Dubois, R., Spindler, G., Brüggemann, E., Ackermann, R., Geyer, A., and Platt, U.: Measurements of Nitrous Acid by DOAS and Diffusion Denuders: A Comparison, in: Proceedings of EUROTRAC Symposium '98: Transport and Chemical Transformation in the Troposphere, Volume I, edited by: Borrell, P. M. and Borrell, P., ISBN 1-85312-743-4, WIT-Press, Southampton, 345–349, 1999.
Pitts Jr., J. N., Grosjean, D., van Cauwenberghe, K., Schmid, J. P., and Fitz, D. R.: Photooxidation of Aliphatic Amines under Simulated Atmospheric Conditions: Formation of Nitrosamines, Nitramines, Amides, and Photochemical Oxidant, Environ. Sci. Technol., 12, 946–953, 1978.
Pitts Jr., J. N., Sanhueza, E., Atkinson, R., Carter, W. P. L., Winer, A. M., Harris, G. W., and Plum, C. N.: An Investigation of the Dark Formation of Nitrous Acid in Environmental Chambers, Int. J. Chem. Kinet., 16, 919–939, 1984.
Ren, X., Harder, H., Martinez, M., Lesher, R. L., Oliger, A., Simpas, J. B., Brune, W. H., Schwab, J. J., Demerjian, K. L., He, Y., Zhou, X., and Gao, H.: OH and $HO_2$ Chemistry in Urban Atmosphere of New York City, Atmos. Envir., 37, 3639–3651, 2003.
Rohrer, F., Brüning, D., Grobler, E. S., Weber, M., Ehhalt, D. H., Neubert, R., Schübler, W., and Levin, L.: Mixing Ratios and Photostationary State of NO and $NO_2$ Observed During the POPCORN Field Campaign at a Rural Site in Germany, J. Atmos. Chem., 31, 119–137, 1998.

Sakamaki, F., Hatakeyama, S., and Akimoto, H.: Formation of Nitrous Acid and Nitric Oxide in the Heterogeneous Dark Reaction of Nitrogen Dioxide and Water Vapour in a Smog Chamber, Int. J. Chem. Kinet., 15, 1013–1029, 1983.
Sakamaki, F. and Akimoto, H.: HONO Formation as Unknown Radical Source in Photochemical Smog Chambers, Int. J. Chem. Kinet., 20, 111–116, 1988.
Saliba, N. A., Yang, H., and Finlayson-Pitts, B. J.: Reaction of Gaseous Nitric Oxide with Nitric Acid on Silica Surfaces in the Presence of Water at Room Temperature, J. Phys. Chem. A, 105, 10 339–10 346, 2001.
Sander, S. P., Friedl, R. R., Golden, D. M., Kurylo, M. J., Huie, R. E., Orkin, V. L., Moortgat, G. K., Ravishankara, A. R., Kolb, C. E., Molina, M. J., and Finlayson-Pitts, B. J.: Chemical Kinetics and Photochemical Data for Use in Stratospheric Modeling, JPL Publication 02-25, Pasadena, California, 2003.
Svensson, R., Ljungström, E., and Lindqvist, O.: Kinetics of the Reaction between Nitrogen Dioxide and Water Vapour, Atmos. Envir., 21, 1529–1539, 1987.
Taira, M. and Kanda, Y.: Continous Generation System for Low-Concentration Gaseous Nitrous Acid, Anal. Chem., 62, 630–633, 1990.
Vogel, B., Vogel, H., Kleffmann, J., and Kurtenbach, R.: Measured and Simulated Vertical Profiles of Nitrous Acid, Part II – Model Simulations and Indications for a Photolytic Source, Atmos. Envir., 37, 2957–2966, 2003.
Wagner, I., Strehlow, H., and Busse, G.: Flash Photolysis of Nitrate Ions in Aqueous Solutions, Z. Phys. Chem., 123, 1–33, 1980.
Wang, L., Milford, J. B., and Carter, W. P. L.: Reactivity Estimates for Aromatic Compounds, Part 1. Uncertainty in Chamber-Derived Parameters, Atmos. Envir., 34, 4337–4348, 2000.
Zhou, X., Beine, H. J., Honrath, R. E., Fuentes, J. D., Simpson, W., Shepson, P. B., and Bottenheim, J. W.: Snowpack Photochemical Production of HONO: a Major Source of OH in the Arctic Boundary Layer in Springtime, Geophys. Res. Lett., 28, 4087–4090, 2001.
Zhou, X., Civerolo, K., Dai, H., Huang, G., Schwab, J., and Demerjian, K.: Summertime Nitrous Acid Chemistry in the Atmospheric Boundary Layer at a Rural Site in New York State, J. Geophys. Res., 107 (D21), 4590, doi:10.1029/2001JD001539, 2002a.
Zhou, X., He, Y., Huang, G., Thornberry, T. D., Carroll, M. A., and Bertman, S. B.: Photochemical Production of Nitrous Acid on Glass Sample Manifold Surface, Geophys. Res. Lett., 29 (14), doi:10.1029/2002GL015080, 2002b.
Zhou, X., Gao, H., He, Y., Huang, G., Bertman, S., Civerolo, K., and Schwab, J.: Nitric Acid Pho-

tolysis on Surfaces in Low-$NO_x$ Environments: Significant Atmospheric Implications, Geophys. Res. Lett., 30 (23), 2217, doi:10.1029/2003GL018620, 2003.

**Table 1.** Detection limit and accuracy of SAPHIR instrumentation used in this analysis.

| Instrument | HONO | NO | $NO_2$ | $O_3$ | Photolysis frequencies |
|---|---|---|---|---|---|
| Detection Limit ($2\sigma$) | 2 pptV | 5 pptV | 10 pptV | 0.5 ppbV | |
| Accuracy | 10% | 5% | 10% | 5% | 10% |
| Time Resolution | 5 min | 90 s | 90 s | 90 s | 2 min |



ACPD
4, 7881–7915, 2004

**Table 2.** Experimental conditions for HONO characterisation experiments; not all experiments are accompanied by LOPAP HONO measurements due to limited availability.

| Experiment Type | Relative Humidity | CO | Initial $NO_2$ | Filter foil | Number of analysed experiments |
|---|---|---|---|---|---|
| A | <1% | 0 | 0 | – | 11 |
| B | >10% | 0 | 0 | – | 9 |
| C | >10% | 550 ppmV | 0 | – | 2 |
| D | >10% | 550 ppmV | 0 | + | 2 |
| E | 30% | 0 | 35 ppbV | – | 1 |



ACPD
4, 7881–7915, 2004

**Table 3.** Reaction scheme used for the model calculation.

| | | | | | |
|---|---|---|---|---|---|
| $O^1D + O_2$ | → | $O_3$ | $NO + O_3$ | → | $NO_2$ |
| $O^1D + N_2$ | → | $O_3$ | $NO + OH$ | → | $HNO_2$ |
| $O^1D + H_2O$ | → | $2{\cdot}OH$ | $NO_2 + NO_3$ | → | $N_2O_5$ |
| $2{\cdot}HO_2$ | → | $H_2O_2$ | $NO_2 + O_3$ | → | $NO_3$ |
| $2{\cdot}HO_2 + H_2O$ | → | $H_2O_2$ | $NO_2 + OH$ | → | $HNO_3$ |
| $CO + OH$ | → | $CO_2 + HO_2$ | $NO_3 + OH$ | → | $HO_2 + NO_2$ |
| $H_2 + OH$ | → | $HO_2$ | $O_3 + OH$ | → | $HO_2$ |
| $H_2O_2 + OH$ | → | $H_2O + HO_2$ | $HNO_2 + h\nu$ | → | $NO + OH$ |
| $HCHO + OH$ | → | $CO + HO_2$ | $H_2O_2 + h\nu$ | → | $2{\cdot}OH$ |
| $HNO_2 + OH$ | → | $H_2O + NO_2$ | $HCHO + h\nu$ | → | $CO + 2{\cdot}HO_2$ |
| $HNO_3 + OH$ | → | $H_2O + NO_3$ | $HCHO + h\nu$ | → | $CO + H_2$ |
| $HO_2 + NO$ | → | $NO_2 + OH$ | $NO_2 + h\nu$ | → | $NO + O_3$ |
| $HO_2 + NO_3$ | → | $NO_2 + OH$ | $NO_3 + h\nu$ | → | $NO$ |
| $HO_2 + O_3$ | → | $OH$ | $NO_3 + h\nu$ | → | $NO_2 + O_3$ |
| $HO_2 + OH$ | → | $H_2O$ | $O_3 + h\nu$ | → | $O^1D$ |
| $N_2O_5$ | → | $NO_2 + NO_3$ | | | |



ACPD

4, 7881–7915, 2004

**Table 4.** Result of fitting the observed time series of NO and $NO_2$ for the experiments mentioned in Table 2 to model calculations using the parameterisation Eq. (1).

| Time period | $a_i$ | $RH_0$ | $T_0$ |
|---|---|---|---|
| July 2001–July 2002 | $4.7\times10^{13}\,cm^{-3}$ | 11.6% | 3950 K |
| August 2002–December 2003 | $8.5\times10^{13}\,cm^{-3}$ | 11.6% | 3950 K |



ACPD
4, 7881–7915, 2004

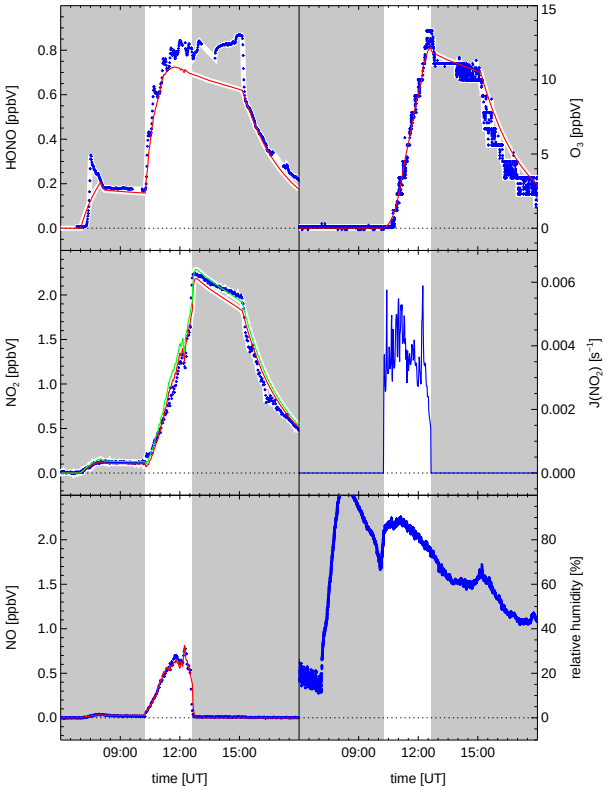


**Fig. 1.** HONO, $NO_x$, and ozone formation in SAPHIR illuminated with sunlight on 8 August 2001 (experiment type B, see Table 2). In the time interval between 07:00 and 08:30 UT, small amounts of HONO and $NO_2$ were flushed into the chamber during the humidification process. Blue symbols mark observations, red and green lines show the result of model calculations (see text).



ACPD
4, 7881–7915, 2004

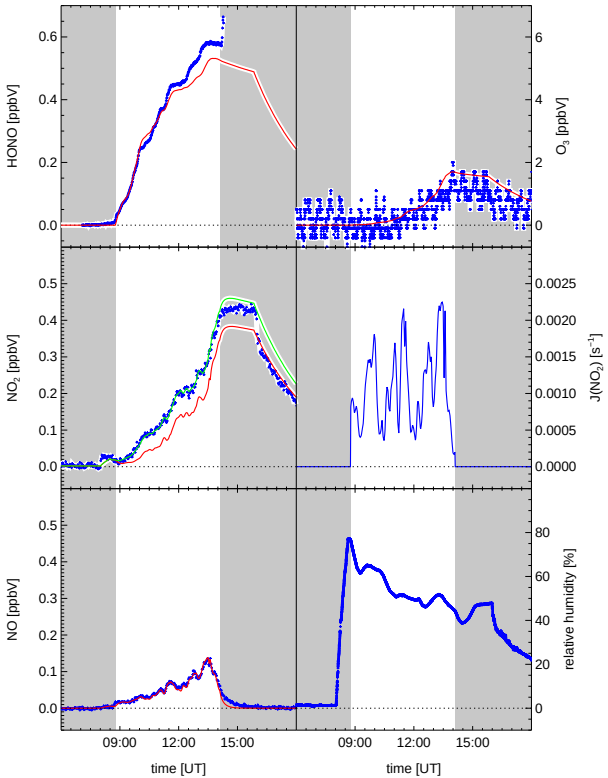


**Fig. 2.** HONO, $NO_x$, and ozone formation in SAPHIR illuminated with sunlight using an additional filter foil in the presence of 550 ppmV of CO on 2 July 2002 (experiment type D, see Table 2). Blue symbols mark observations, red and green lines show the result of model calculations (see text).



ACPD
4, 7881–7915, 2004

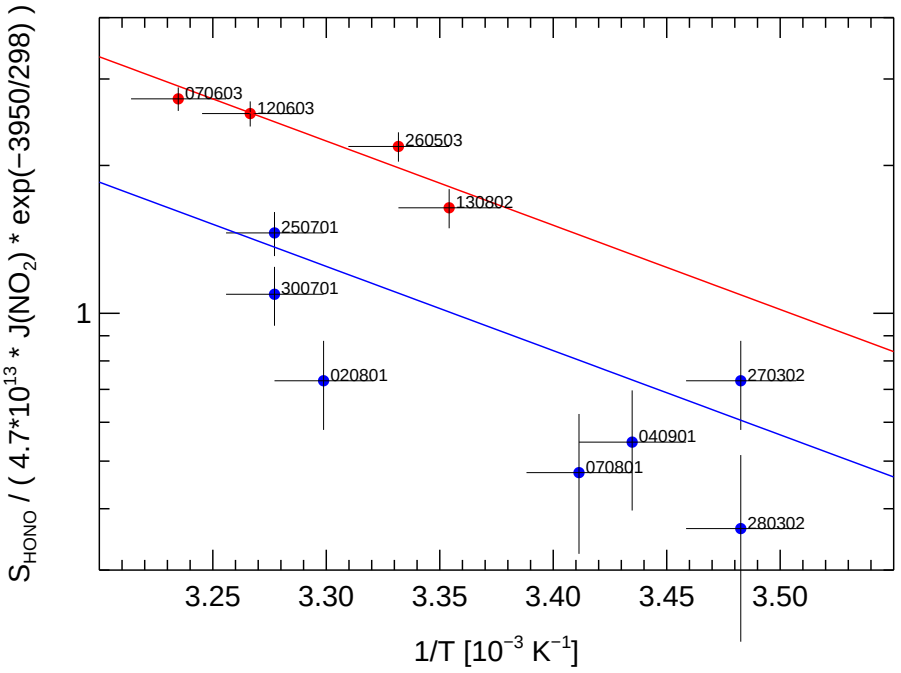


**Fig. 3.** Dependence of $S(HONO)_{SAPHIR}$ on 1/T determined from the fit of Eq. (1) to observed time series of NO and $NO_2$ for the experiments type A in Table 2 with relative humidities below 1%. Indicated is the date of experiments in the form DDMMYY. $S(HONO)_{SAPHIR}$ has been scaled with $J(NO_2)$. The blue dots mark experiments before August 2002, the red dots those after that date. The blue and red lines represent Eq. (1) with parameters given in Table 4.



ACPD
4, 7881–7915, 2004

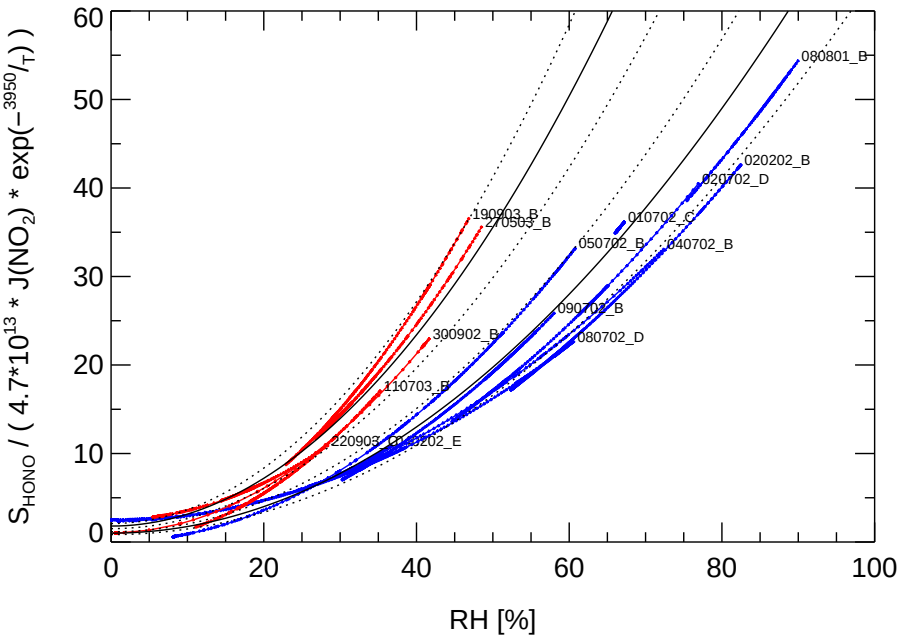


**Fig. 4.** Dependence of $S(HONO)_{SAPHIR}$ on relative humidity determined from the fit of Eq. (1) to observed time series of NO and $NO_2$ for experiments B, C, D, and E mentioned in Table 2 with relative humidities above 10%. Indicated is the date of experiments in the form DDMMYY and the type of experiment. $S(HONO)_{SAPHIR}$ has been scaled with $J(NO_2)$ and the temperature function in Eq. (1) to separate the dependence on relative humidity. Blue lines mark experiments before 13 August 2002, red lines those after that date. The solid black lines represent Eq. (1) with parameters given in Table 4. Dotted black lines indicate a region of ±0.15× ordinate value above and below the solid black line. This region is defined by the spread of the individual experiments belonging to each of the two groups.

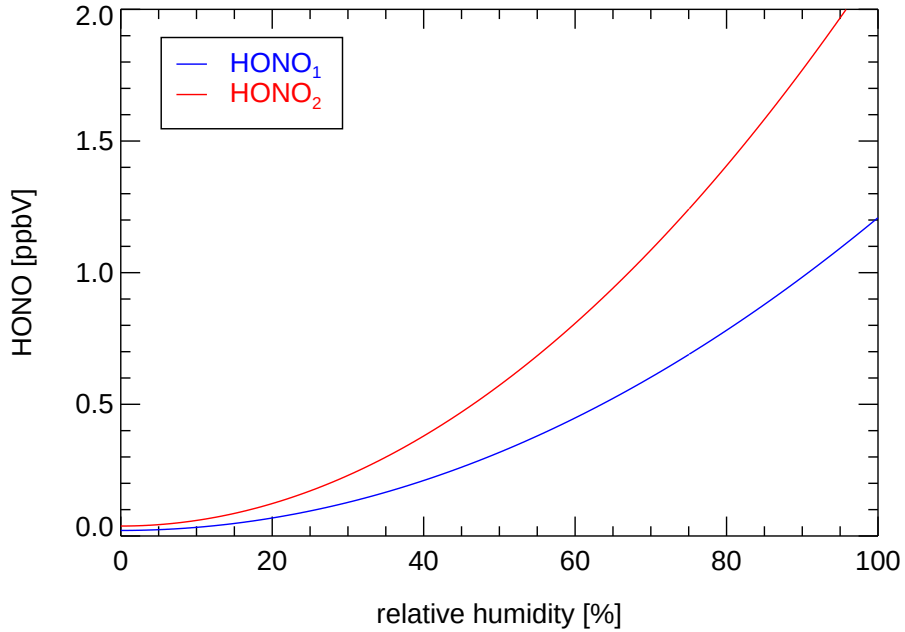


**Fig. 5.** Predicted stationary HONO mixing ratios inside SAPHIR calculated with Eq. (1) and parameters from Table 4 for T=295 K.



ACPD
4, 7881–7915, 2004

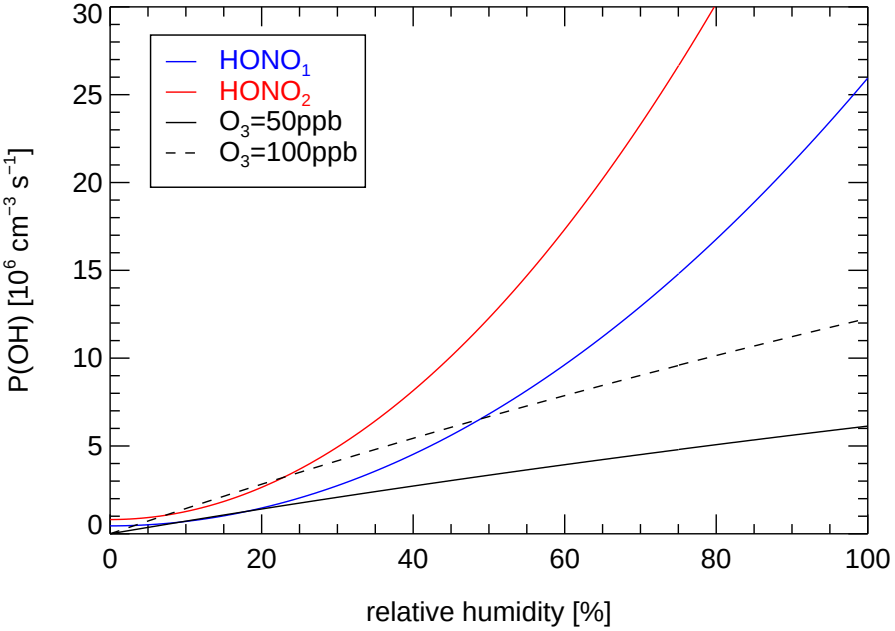


**Fig. 6.** Production of OH radicals inside SAPHIR from HONO photolysis and from ozone photolysis calculated with Eqs. (1), (5), and (6) and parameters from Table 4 for T=295 K, $J(NO_2)=5\times10^{-3}\,s^{-1}$, and $J(O^1D)=1.5\times10^{-5}\,s^{-1}$.



ACPD
4, 7881–7915, 2004